

Multi-Mapping Image-to-Image Translation with Central Biasing Normalization

Xiaoming Yu, Zhenqiang Ying, *Student Member, IEEE*, Thomas Li, Shan Liu, and Ge Li, *Member, IEEE*,

Abstract—Image-to-image translation is a class of image processing and vision problems that translates an image to a different style or domain. To improve the capacity and performance of one-to-one translation models, multi-mapping image translation have been attempting to extend them for multiple mappings by injecting latent code. Through the analysis of the existing latent code injection models, we find that latent code can determine the target mapping of a generator by controlling the output statistical properties, especially the mean value. However, we find that in some cases the normalization will reduce the consistency of same mapping or the diversity of different mappings. After mathematical analysis, we find the reason behind that is that the distributions of same mapping become inconsistent after batch normalization, and that the effects of latent code are eliminated after instance normalization. To solve these problems, we propose consistency within diversity design criteria for multi-mapping networks. Based on the design criteria, we propose central biasing normalization (CBN) to replace existing latent code injection. CBN can be easily integrated into existing multi-mapping models, significantly reducing model parameters. Experiments show that the results of our method is more stable and diverse than that of existing models.

Index Terms—Normalization, multiple mappings, latent code injection, image-to-image translation.

I. INTRODUCTION

MANY image processing and computer vision problems can be framed as image-to-image translation tasks [1], such as facial attributes transform, grayscale image colorization and edge maps to photos. This can also be viewed as mapping an image from one specific domain to another. Although many studies have shown remarkable success in image-to-image translation between two domains, *e.g.* supervised image translation [1], [2] and unsupervised image translation [3]–[6], these one-to-one mapping methods are not suitable for multi-mapping problems. In these methods, the generated model tries to learn a specific mapping from the source domain to the target domain. It means that different models need to

This work was supported by the Project of National Engineering Laboratory for Video Technology-Shenzhen Division, Shenzhen Municipal Science and Technology Program under Grant (JCYJ20170818141146428), and National Natural Science Foundation of China and Guangdong Province Scientific Research on Big Data (No. U1611461). This paper was recommended by Associate Editor X. XX.

X. Yu, Z. Ying, T. Li and G. Li are with the School of Electronic and Computer Engineering, Shenzhen Graduate School, Peking University, 518055 Shenzhen, China (e-mail: xiaomingyu@pku.edu.cn; zqying@pku.edu.cn; thomasli@pkusz.edu.cn geli@ece.pku.edu.cn). S. Liu is with the Media Lab, Tencent (e-mail: shanli@tencent.com).

Color versions of one or more of the figures in this paper are available online at <http://ieeexplore.ieee.org>.

Digital Object Identifier XX.XXXX/XXX.20XX.XXXXXXX

Manuscript received XXX XX, 20XX; revised XXX XX, 20XX.

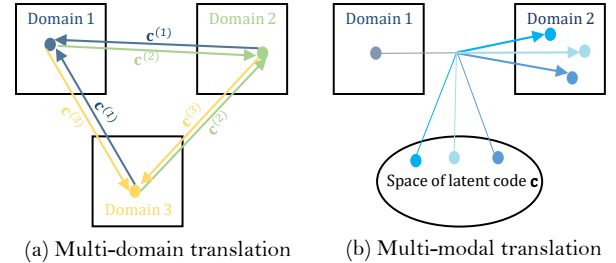


Fig. 1. An illustration of multi-mapping indicated by latent code c . (a) Multi-domain translation indicated by limited domain latent code. (b) Cross-domain translation indicated by potential attribute latent code.

be built for different pairs of mapping, even though some mappings share common semantics. To address this problem, the multi-mapping image-to-image translation has received more and more attention [7]–[9]. In these methods, latent code is introduced to indicate different mappings, and applied to multi-domain translation tasks [7], [8] and multi-modal translation tasks [9].

For multi-domain translation, the domain labels (*e.g.* binary or one-hot vector) are often used as latent code to represent the domain information. Given training data from several different domains, multi-domain models learn to translate images from one domain to another domain indicated by the latent code. As illustrated in Fig. 1(a), there are three possible latent code corresponding to three target domains. As shown in Fig. 2(a), different hair colors represent different domains in this multi-domain translation tasks.

For multi-modal translation, the latent code is usually sampled from a latent space with prior distribution (*e.g.* Uniform or Gaussian priors) to indicate the target modal, as shown in Fig. 1(b). In these cases, the latent code reflects intra-domain diversity for cross-domain translation such as edge-to-photos, labels-to-photos and night-to-day, as shown in Fig. 2(b).

To capture the joint output distribution between input image and latent code, existing convolution based methods [7]–[9] inject the latent code to the generator by replicating it to the size of the convolutional input. Although these methods show some impressive results, there are two some unsolved problems. First, due to the lack of theoretical analysis, it is hard to understand how the latent code works in multi-mapping translation. Second, existing latent code injection (LCI) models work well in their default configuration, but are sensitive to the choice of network structure, *e.g.* length of latent code, padding strategies, or normalization operations. So it is significant to explore the role of latent code and the

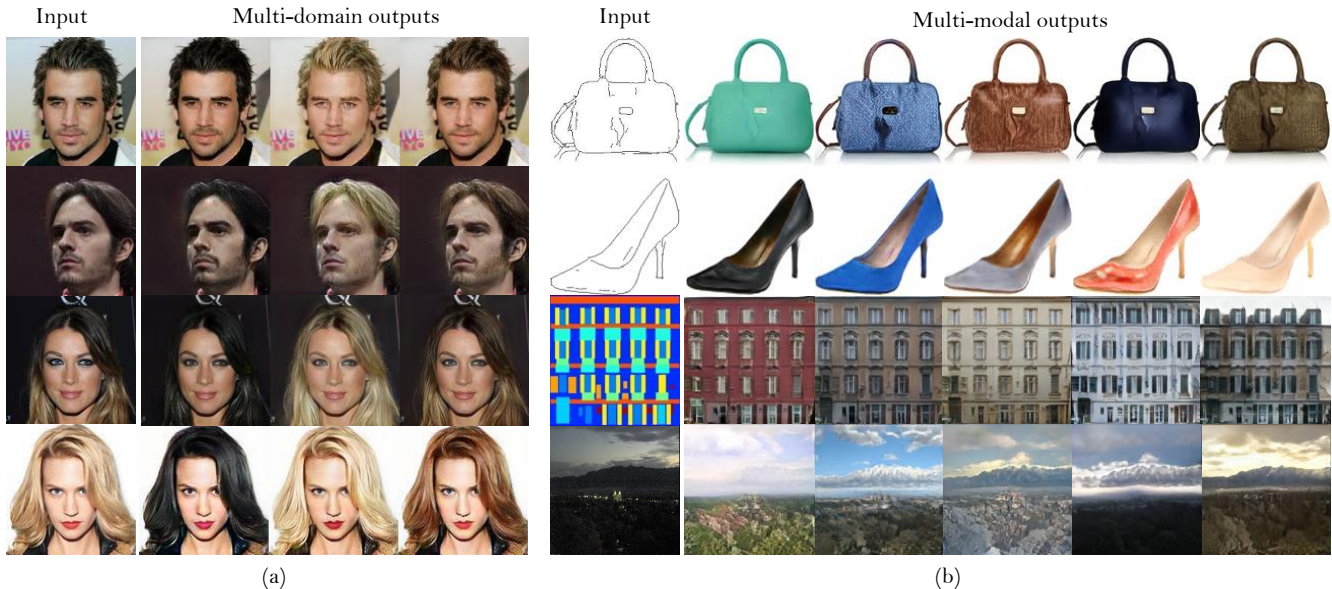


Fig. 2. Multi-mapping image-to-image translation tasks. (a) The multi-domain translation results of different hair colors (black, blond, brown). (b) The cross-domain translation with multi-modal results. The first two rows present the `edge2photo` translation task, next row is the `label2photo` task and remaining is the `night2day` task. The results in same task are generated by a single generator with central biasing normalization.

effect of injection method.

Through mathematical analysis, we find that the latent code can control the target mapping by affecting the mean value of convolutional outputs. Besides, we find that the batch normalization will cause *mapping inconsistency* for different instances of same mapping, and the instance normalization will cause *mapping indistinguishability* for different mappings. Therefore, we propose the *consistency within diversity design criteria* for solving these problems. With the *design criteria*, we propose central biasing normalization as an alternative method for injecting the latent code in multi-mapping model. By replacing the existing LCI generator with the *central biasing generator*, we show that our method can stably adjust the distribution of the outputs.

In summary, this paper makes the following contributions:

- We derive that the role of latent code in multi-mapping tasks is to control the mean value of the feature maps after convolution in Section III.
- As far as we know, we are the first to point out the potential problems of common latent code injection and to propose the *consistency within diversity criteria*, as shown in Section IV.
- Based on the *design criteria*, we propose central biasing normalization as an alternative method of injecting latent code in Section V.

II. RELATED WORK

Benefiting from large public image repositories and high-performance computing systems, convolutional neural networks (CNNs) have been widely used in various image processing problems in recent years. By minimizing the loss function that evaluates the quality of results, CNNs attempt to model the mapping between the source and target domain.

However, it is difficult to manually design an effective and universal loss function for different tasks. To overcome this problem, recent studies apply generative adversarial networks (GANs) since they use a loss function that adapts to the data instead of the specific evaluation.

A. Generative Adversarial Networks

By staging a zero-sum game, GANs have shown impressive results in image generation [10]–[15]. The extensions of GANs with conditional settings have achieved impressive results in various conditional generation tasks such as image inpainting [16], super-resolution [17], text2image [18], multi-view synthesis[19], and image editing [20].

B. Image-to-Image Translation using GANs

Encouraged by the development of GANs and conditional GANs (cGANs), previous studies focused on paired [1] and unpaired image-to-image translation tasks [3]–[6]. Pix2pix [1] uses cGANs [21] to perform supervised learning with data pairs. CycleGAN [3], DiscoGAN [5], and DualGAN [4]

TABLE I
MODEL COMPARISON OF IMAGE-TO-IMAGE TRANSLATION

Model	Paired Data	Multi-Domain	Multi-Modal	Main Idea
Pix2pix	Need	×	×	Conditional GANs
CycleGAN	No need	×	×	Cycle consistency
DiscoGAN	No need	×	×	Discover cross-domain relations
DualGAN	No need	×	×	Dual learning
UNIT	No need	×	×	Shared latent space assumption
Fader Networks	No need	✓	×	Invariant latent representation
StarGAN	No need	✓	×	Auxiliary classifier
BicycleGAN	Need	×	✓	Bijjective consistency

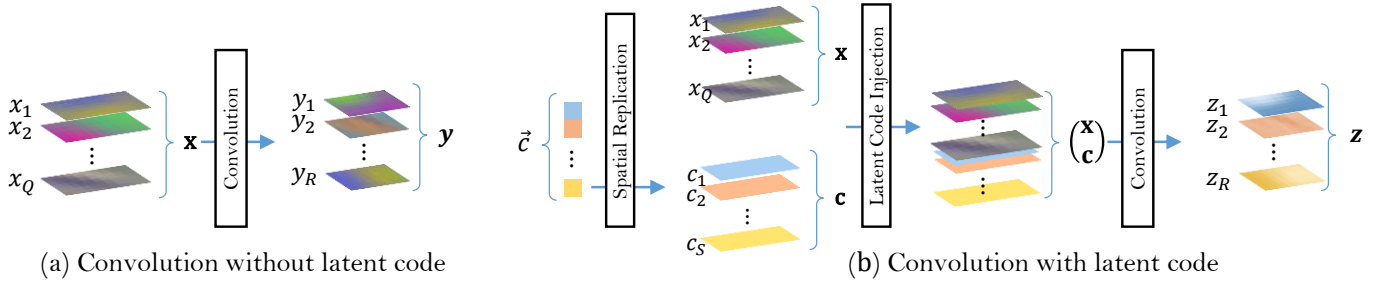


Fig. 3. Convolution operation without/with latent code. (a) The common convolution without latent code. (b) The convolution with latent code injection.

enforce cycle consistency for unpaired image-to-image translation. UNIT [6] combines variational autoencoders [22] with CoGAN [23] to learn a joint distribution of images in different domains. These studies have promoted the development of one-to-one mapping image translation, but have shown limited scalability for multi-mapping translation.

C. Multi-Mapping Translation

To achieve a more scalable approach for image-to-image translation, researchers recently have made significant progress in the development of multi-mapping translation [7]–[9], as compared in Table I. For instance, StarGAN [8] uses a single model and latent code to achieve multiple domain image-to-image translations. It trains the generator with the discriminator that combines with an auxiliary classifier [24], which encourages the learning of multi-mapping indicated by the latent code. Fader Networks [7] use the attribute-invariant representations, encoded by the input image, and the latent code for image reconstruction. BicycleGAN [9] combines VAE-GAN objects [25] and LR-GAN objects [12], [26], [27] for a bijective mapping between the latent code and output spaces. The common feature of these tasks is that they learn a joint distribution between input images and latent code, so it is important to use the latent code in a reasonable way.

D. Latent Code for Multi-Mapping

For controlling multiple attributes of the generated image, a meaningful vector \vec{c} , called latent code, is introduced for targeting the salient structured semantic features. For instance, when generating a facial image, the latent code \vec{c} will indicate the features we need, like the gender or the hair color or the expression. In existing multi-mapping models [7]–[9], latent code \vec{c} is injected by spatial replication and concatenation into the input of a convolutional neural network. Although existing methods show some impressive results, latent code injection in these methods is unreliable and may lead to mode collapse. We discuss this problem in Section IV and compare our method with StarGAN and BicycleGAN in Section VI.

III. COMMON LATENT CODE INJECTION

In this section, we will explore how existing latent code injection works in multi-mapping models by modeling its interaction with convolution kernels during convolution. We

will also revisit the normalization to facilitate the later analysis in Sect. IV.

A. Convolution Operation without Latent Code

Following the notation of Convolutional Matrix Multiplication [28], we extend the matrix of numbers to the matrix of feature maps or convolution kernels. Here, each element is a feature map or a convolution kernel instead of a number.

Let x_1, x_2, \dots, x_Q be the Q input feature maps (each sized $M \times N$) and $w_{r,q}$ be the $R \times Q$ convolution kernels (each sized $K \times L$) where $r = 1, 2, \dots, R$ and $q = 1, 2, \dots, Q$. Then the R output feature maps y_1, y_2, \dots, y_R can be represented as

$$\begin{aligned} y_1 &= w_{1,1} * x_1 + w_{1,2} * x_2 + \dots + w_{1,Q} * x_Q \\ y_2 &= w_{2,1} * x_1 + w_{2,2} * x_2 + \dots + w_{2,Q} * x_Q \\ &\vdots \\ y_R &= w_{R,1} * x_1 + w_{R,2} * x_2 + \dots + w_{R,Q} * x_Q, \end{aligned} \quad (1)$$

where $*$ is the convolution operation. Further, these equations can be redefined as a special matrix/vector multiplication

$$\mathbf{y} = \mathbf{W} \times \mathbf{x}, \quad (2)$$

where $\mathbf{x} = (x_1, x_2, \dots, x_Q)^T$, $\mathbf{y} = (y_1, y_2, \dots, y_R)^T$, and

$$\mathbf{W} = \begin{pmatrix} w_{1,1} & w_{1,2} & \dots & w_{1,Q} \\ w_{2,1} & w_{2,2} & \dots & w_{2,Q} \\ \vdots & \vdots & \ddots & \vdots \\ w_{R,1} & w_{R,2} & \dots & w_{R,Q} \end{pmatrix}.$$

B. Convolution Operation with Latent Code

As shown in Fig.3, we denote the special vector \mathbf{c} as the S latent code feature maps, where $\mathbf{c} = (c_1, c_2, \dots, c_S)^T$. The element of \mathbf{c} is replicated from the numerical element of original latent code \vec{c}

$$c_s(m, n) = \vec{c}_s,$$

where $s = 1, 2, \dots, S$; $m = 1, 2, \dots, M$; $n = 1, 2, \dots, N$ and c_s is a constant feature map in which every element has same value. We denote $v_{r,s}$ as the $R \times S$ convolution kernel that is associated with the latent code. Then

$$\mathbf{o} = \mathbf{V} \times \mathbf{c}, \quad (3)$$

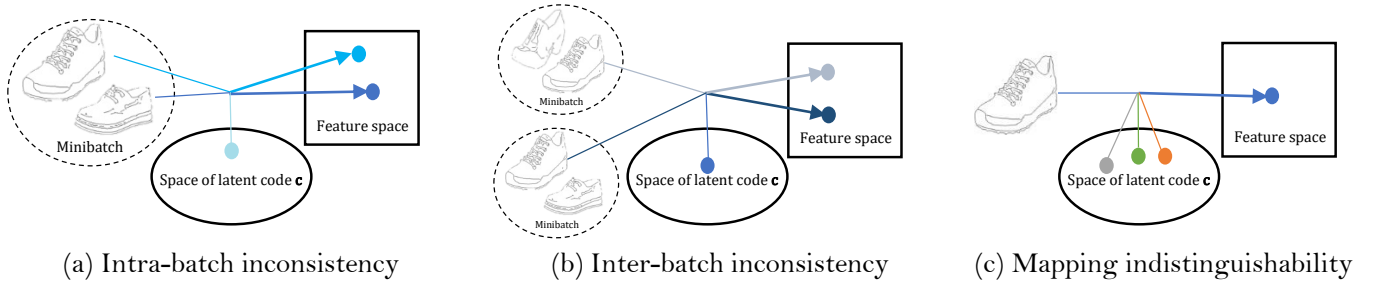


Fig. 4. The potential problems of existing LCI models. (a) The intra-batch inconsistency problem of BN. (b) The inter-batch inconsistency problem of BN. (c) The Mapping indistinguishable problem of IN.

where $\mathbf{c} = (c_1, c_2, \dots, c_S)^T$, $\mathbf{o} = (o_1, o_2, \dots, o_R)^T$, and

$$\mathbf{V} = \begin{pmatrix} v_{1,1} & v_{1,2} & \cdots & v_{1,S} \\ v_{2,1} & v_{2,2} & \cdots & v_{2,S} \\ \vdots & \vdots & \ddots & \vdots \\ v_{R,1} & v_{R,2} & \cdots & v_{R,S} \end{pmatrix}.$$

Note each feature map o_r is a constant channel as it is the linear combination of feature maps from \mathbf{c} :

$$o_r = v_{r,1} * c_1 + v_{r,2} * c_2 + \cdots + v_{r,S} * c_S. \quad (4)$$

The whole convolution operation from input \mathbf{x} and \mathbf{c} can be represented as

$$\mathbf{z} = (\mathbf{W}, \mathbf{V}) \times \begin{pmatrix} \mathbf{x} \\ \mathbf{c} \end{pmatrix} = \mathbf{y} + \mathbf{o}, \quad (5)$$

where $\mathbf{z} = (z_1, z_2, \dots, z_R)^T$ is the final convolution output.

We make two observations about the convolution with latent code. First, the final convolution output \mathbf{z} can be decomposed into two separate parts \mathbf{y} and \mathbf{o} . It means that the target mapping is only determined by the latent code \mathbf{c} . Second, different latent code only provide different offsets to the output feature maps. In other words, the network needs to distinguish between different mappings based on the mean value of feature maps.

C. Normalization

1) *Batch Normalization*: To accelerate training and improve the performance of deep networks, Ioffe and Szegedy introduced batch normalization (BN) [29] to reduce the internal covariate shift [30] of networks by normalizing the feature statistics. Although BN is designed to ease the training of discriminative networks, it is also effective in deep generative models [15]. In the training stage, the input minibatch mean and variance are used to normalize each feature map of the convolutional output:

$$\text{BN}(z_r) = \frac{z_r - \mathbb{E}[Z_r]}{\sqrt{\text{Var}[Z_r]}}, \quad (6)$$

where $Z_r = (z_r^{(1)}, z_r^{(2)}, \dots)$ is the batch of r -th feature map. During the inferencing stage, BN replaces the minibatch statistics with moving statistics.

2) *Instance Normalization*: In style transfer tasks, Ulyanov *et al.* [31] find that critical improvement could be achieved by replacing batch normalization with instance normalization (IN). Recent image transform tasks [3], [8], [9] confirmed that IN is also useful for improving the quality of transform results. Unlike BN that uses mini-batch statistics, IN only uses the statistics of the instance itself for normalization:

$$\text{IN}(z_r) = \frac{z_r - \mathbb{E}[z_r]}{\sqrt{\text{Var}[z_r]}}. \quad (7)$$

Consequently, the feature statistics IN uses are consistent between the training and inference stages.

3) *Scale and Shift*: A simple normalization operation $\text{Norm}(\cdot)$ for convolution output may change what it can represent. Therefore, the affine parameters γ_r , and β_r are used for restoring the representation power of the network:

$$\hat{z}_r = \gamma_r \text{Norm}(z_r) + \beta_r. \quad (8)$$

IV. ANALYSIS OF PROBLEMS WITH COMMON LCI

According to the analysis in the above section, we know the role of the latent code is to provide a constant offset for output feature maps. In this section, we will use some examples to explain how normalization confuses the statistical mean of output feature map and degrades the model performance. Then, we will present *consistency within diversity criteria* to guide the designing of the multi-mapping model.

A. Impaired Consistency of Batch Normalization

1) *Intra-batch Inconsistency*: Consider this minibatch $\mathbf{Z}^{(1)} = (\mathbf{z}^{(1)}, \mathbf{z}^{(2)}, \mathbf{z}^{(3)})$, where

$$\begin{aligned} \mathbf{z}^{(1)} &= (\mathbf{W}, \mathbf{V}) \times \begin{pmatrix} \mathbf{x}^{(1)} \\ \mathbf{c}^{(1)} \end{pmatrix} = \mathbf{y}^{(1)} + \mathbf{o}^{(1)}, \\ \mathbf{z}^{(2)} &= (\mathbf{W}, \mathbf{V}) \times \begin{pmatrix} \mathbf{x}^{(2)} \\ \mathbf{c}^{(1)} \end{pmatrix} = \mathbf{y}^{(2)} + \mathbf{o}^{(1)}, \\ \mathbf{z}^{(3)} &= (\mathbf{W}, \mathbf{V}) \times \begin{pmatrix} \mathbf{x}^{(3)} \\ \mathbf{c}^{(1)} \end{pmatrix} = \mathbf{y}^{(3)} + \mathbf{o}^{(1)}. \end{aligned} \quad (9)$$

In batch $\mathbf{Z}^{(1)}$, different input instances $\mathbf{x}^{(1)}, \mathbf{x}^{(2)}, \mathbf{x}^{(3)}$ map to the same domain indicated by latent code $\mathbf{c}^{(1)}$. It implies that the distribution of instances in $\mathbf{Z}^{(1)}$ should be similar in the feature space. But without any distribution alignment

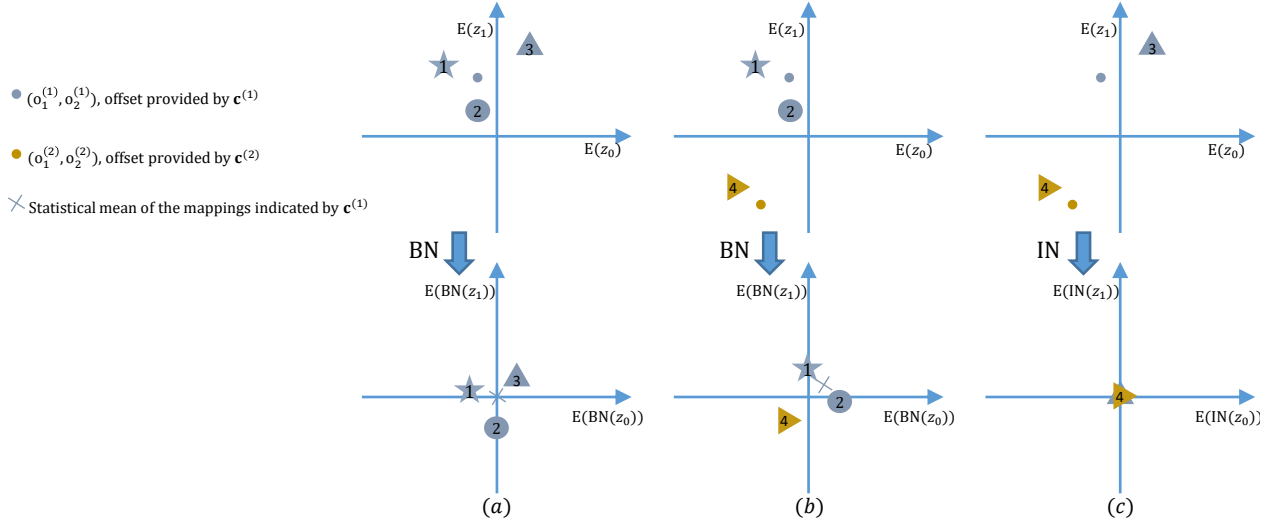


Fig. 5. A toy visualization in which only two dimensions are shown for potential problems of LCI model. The first row in these sub-figure is the output of convolution with normalization. The second row is the output with different normal operations. It should be noticed the location of $\mathbf{z}^{(3)}$ is the same as $\mathbf{z}^{(4)}$ in the second row of the last sub-figure.

operations, the statistical mean of feature is inconsistent in different instances

$$\begin{aligned} & \mathbb{E}[\text{BN}(z_r^{(1)})] - \mathbb{E}[\text{BN}(z_r^{(2)})] \\ &= \mathbb{E}[\text{BN}(z_r^{(1)}) - \text{BN}(z_r^{(2)})] \\ &= \mathbb{E}\left[\frac{z_r^{(1)} - z_r^{(2)}}{\sqrt{\text{Var}[Z_r^{(1)}]}}\right] \end{aligned} \quad (10)$$

Since $z_r^{(1)} = y_r^{(1)} + o_r^{(1)}$ and $z_r^{(2)} = y_r^{(2)} + o_r^{(1)}$. Hence

$$\begin{aligned} & \mathbb{E}[\text{BN}(z_r^{(1)})] - \mathbb{E}[\text{BN}(z_r^{(2)})] \\ &= \frac{\mathbb{E}[y_r^{(1)} - y_r^{(2)}]}{\sqrt{\text{Var}[Z_r^{(1)}]}}. \end{aligned} \quad (11)$$

In most cases we have $\mathbb{E}[y_r^{(1)}] \neq \mathbb{E}[y_r^{(1)} y_r^{(2)}]$, i.e., $\mathbb{E}[y_r^{(1)} - y_r^{(2)}] \neq 0$, therefore

$$\mathbb{E}[\text{BN}(z_r^{(1)})] \neq \mathbb{E}[\text{BN}(z_r^{(2)})]. \quad (12)$$

Similarly, we can derive $\mathbb{E}[\text{BN}(z_r^{(1)})] \neq \mathbb{E}[\text{BN}(z_r^{(2)})] \neq \mathbb{E}[\text{BN}(z_r^{(3)})]$, as illustrated in Fig. 4(a) and 5(a). Although these three instances have the same mapping, their statistical mean is inconsistent. We call this phenomenon *intra-batch inconsistency*. This inconsistency is considered to be the shortcoming of BN in style transfer tasks [32].

2) *Inter-batch Inconsistency*: Replace $\mathbf{z}^{(3)}$ in $\mathbf{Z}^{(1)}$ with $\mathbf{z}^{(4)}$, where

$$\mathbf{z}^{(4)} = (\mathbf{W}, \mathbf{V}) \times \begin{pmatrix} \mathbf{x}^{(3)} \\ \mathbf{c}^{(2)} \end{pmatrix} = \mathbf{y}^{(3)} + \mathbf{o}^{(2)}. \quad (13)$$

The new batch is $\mathbf{Z}^{(2)} = (\mathbf{z}^{(1)}, \mathbf{z}^{(2)}, \mathbf{z}^{(4)})$. Here, we use the statistical mean of the same mapping instances to represent the main characteristic of a specific mapping. In batch $\mathbf{Z}^{(1)}$, the statistical mean of the mapping indicated by $\mathbf{c}^{(1)}$ is

$\mathbb{E}[\text{BN}(\mathbf{Z}^{(1)})] = 0$, but the mean value indicated by $\mathbf{c}^{(1)}$ in batch $\mathbf{Z}^{(2)}$ is

$$\begin{aligned} & \mathbb{E}[(\text{BN}(z_r^{(1)}), \text{BN}(z_r^{(2)}))] \\ &= \frac{1}{2} \mathbb{E}[\text{BN}(z_r^{(1)})] + \frac{1}{2} \mathbb{E}[\text{BN}(z_r^{(2)})] \\ &= \frac{\mathbb{E}[z_r^{(1)}] + \mathbb{E}[z_r^{(2)}] - 2\mathbb{E}[Z_r^{(2)}]}{2\sqrt{\text{Var}[Z_r^{(2)}]}}. \end{aligned} \quad (14)$$

Since $\mathbb{E}[Z_r^{(2)}] = \frac{1}{3}\mathbb{E}[z_r^{(1)}] + \frac{1}{3}\mathbb{E}[z_r^{(2)}] + \frac{1}{3}\mathbb{E}[z_r^{(3)}]$. Hence

$$\begin{aligned} & \mathbb{E}[(\text{BN}(z_r^{(1)}), \text{BN}(z_r^{(2)}))] \\ &= \frac{\mathbb{E}[Z_r^{(2)}] - \mathbb{E}[z_r^{(3)}]}{2\sqrt{\text{Var}[Z_r^{(2)}]}} \\ &= -\frac{1}{2} \mathbb{E}[\text{BN}(z_r^{(3)})]. \end{aligned} \quad (15)$$

In most cases, $\mathbb{E}[\text{BN}(z_r^{(3)})] \neq 0$. Therefore, the mean value of same mapping is always inconsistent between different batches. It means that the inconsistency also exists between different batches in the training stage, as shown in Fig. 4(b) and 5(a,b). We call this phenomenon *inter-batch inconsistency*. To address this, the uniform sampling of different mappings is required for each training minibatch, which is difficult when there are a lot of mappings.

Due to the existence of the above phenomenon, the network has to continuously adapt to a new distribution to distinguish between different mappings in training stage. Therefore, the network will suffer from covariate shift [30] which reduces its performance. We call these problems *mapping inconsistency*.

B. Impaired Diversity of Instance Normalization

The *mapping inconsistency* of BN is caused by normalizing the feature statistics of a minibatch, and IN does not have this problem since it normalizes the feature statistics of an instance.

But IN will eliminate the diversity indicated by the latent code, as illustrated in Fig. 4(c) and 5(c).

Consider these two instances $\mathbf{z}^{(3)}$ and $\mathbf{z}^{(4)}$. With the same input $\mathbf{x}^{(3)}$, different mappings are indicated by $\mathbf{c}^{(1)}$ and $\mathbf{c}^{(2)}$. After IN

$$\begin{aligned}
 & \text{IN}(z_r^{(3)}) - \text{IN}(z_r^{(4)}) \\
 &= \frac{y_r^{(3)} + o_r^{(1)} - \mathbb{E}[y_r^{(3)} + o_r^{(1)}]}{\sqrt{\text{Var}[y_r^{(3)} + o_r^{(1)}]}} - \frac{y_r^{(3)} + o_r^{(2)} - \mathbb{E}[y_r^{(3)} + o_r^{(2)}]}{\sqrt{\text{Var}[y_r^{(3)} + o_r^{(2)}]}} \\
 &= \frac{y_r^{(3)} - \mathbb{E}[y_r^{(3)}]}{\sqrt{\text{Var}[y_r^{(3)}]}} - \frac{y_r^{(3)} - \mathbb{E}[y_r^{(3)}]}{\sqrt{\text{Var}[y_r^{(3)}]}} = 0, \\
 &\Rightarrow \text{IN}(z_r^{(3)}) = \text{IN}(z_r^{(4)}).
 \end{aligned} \tag{16}$$

Since o_r is the constant feature map, the diversity indicated by latent code will be eliminated after IN, as shown in Eq. 16. It means that the model cannot distinguish different mappings indicated by latent code. We call this problem *mapping indistinguishability*.

C. Consistency Within Diversity Criteria

With these potential problems, the common LCI model has difficulty in learning the stable mapping indicated by latent code. Motivated by the role of latent code, we argue that the feature statistics, especially the mean value of feature map, represents the target mapping. Therefore, we propose the *consistency within diversity criteria* to help model multi-mapping. The basic goal is to reduce mapping inconsistency while maintaining diversity. We define the multi-mapping result as $\phi(\mathbf{x}, \vec{c})$, where \vec{c} is the original latent code.

1) *Consistency criterion*: To reduce mapping inconsistency, different $\mathbf{x}^{(1)}$ and $\mathbf{x}^{(2)}$ should produce consistent outputs when given same latent code \vec{c} .

$$\mathbb{E}[\phi(\mathbf{x}^{(1)}, \vec{c})] = \mathbb{E}[\phi(\mathbf{x}^{(2)}, \vec{c})]. \tag{17}$$

It means that the statistical mean of the mapping function $\phi(\mathbf{x}, \vec{c})$ should not related to the input \mathbf{x} .

2) *Diversity criterion*: To maintain diversity, same input \mathbf{x} should produce diversity outputs when given different $\vec{c}^{(1)}$ and $\vec{c}^{(2)}$. Therefore, the mean value of the outputs should not be identical:

$$\mathbb{E}[\phi(\mathbf{x}, \vec{c}^{(1)})] \neq \mathbb{E}[\phi(\mathbf{x}, \vec{c}^{(2)})]. \tag{18}$$

In other words, the statistical mean of the mapping function $\phi(\mathbf{x}, \vec{c})$ should related to the input \vec{c} .

V. PROPOSED METHOD BASED ON CENTRAL BIASING NORMALIZATION

In this section, we first propose the central biasing operation for common normalization to meet the *design criteria*. Then we apply the proposed central biasing normalization (CBN) to construct our central biasing generator (CBG) for multi-mapping translation.

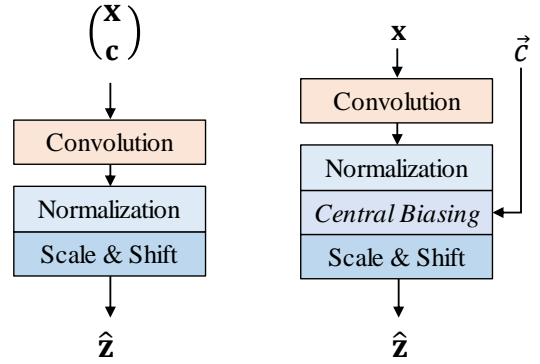


Fig. 6. Left: a traditional convolutional block with latent code injection. Right: a convolutional block with proposed central biasing normalization.

A. Central Biasing Normalization

1) *Formulation*: We first eliminate the offset of normalization feature maps to meet the consistency criterion, which aligns the distribution center of different instances. Then we append a bias calculated by latent code to the distribution center and meet the diversity criterion. So we call this method as central biasing normalization. it can be represented as

$$\text{CBN}(y_r, \vec{c}) = \text{Norm}(y_r) - \mathbb{E}[\text{Norm}(y_r)] + b_r(\vec{c}), \tag{19}$$

$$b_r(\vec{c}) := \tanh(f(\vec{c})), \tag{20}$$

where $\text{Norm}(\cdot)$ represents the common normalization and $b_r(\vec{c})$ is the bias for r -th output feature map, which is initialized simply by applying an affine transformation f to the latent code. Using this initialized bias $f(\vec{c})$ also meets the *design criteria*, but we argue that violates the original intention of normalization. The normalization operation is introduced to accelerate deep network training [29]. It can reduce the internal covariate shift of the network by ensuring the input distribution is stable for the next layer. But without any constraints, the feature distribution after adding bias $f(\vec{c})$ is unknown since there is no constraint on the range of bias. To stabilize the output distribution, we append a \tanh function to constrain range of bias. The final bias for feature map is defined as Eq. 20.

The mean value of feature is $\mathbb{E}[\text{CBN}(y_r, \vec{c})] = b_r(\vec{c})$, where $b_r(\vec{c}) \in [-1, 1]$. With the scale and shift operation, the distribution after normalization is stable for the next layer.

2) *Proof*: Without the central biasing, batch normalization does not meet the consistency criterion.

$$\begin{aligned}
 \mathbb{E}[\text{BN}(z_r)] &= \mathbb{E}\left[\frac{z_r - \mathbb{E}[Z_r]}{\sqrt{\text{Var}[Z_r]}}\right] = \frac{\mathbb{E}[z_r] - \mathbb{E}[Z_r]}{\sqrt{\text{Var}[Z_r]}} \\
 &= \frac{\mathbb{E}[y_r + o_r] - \mathbb{E}[Y_r + O_r]}{\sqrt{\text{Var}[Z_r]}} \\
 &= \frac{\mathbb{E}[y_r + o_r] - \mathbb{E}[Y_r + O_r]}{\sqrt{\text{Var}[Z_r]}} \\
 &= \frac{\mathbb{E}[y_r - \mathbb{E}[Y_r]]}{\sqrt{\text{Var}[Z_r]}} + \frac{\mathbb{E}[o_r - \mathbb{E}[O_r]]}{\sqrt{\text{Var}[Z_r]}}.
 \end{aligned} \tag{21}$$

TABLE II

THE NETWORK ARCHITECTURE OF CBG. “ $C \times K \times L$ CONV $S_n P_m$ ” DENOTES C n -STRIDE CONVOLUTIONAL FILTERS WITH $K \times L$ KERNEL SIZE AND m SIZED ZERO-PADDING OR REFLECTION-PADDING. H AND W ARE THE HEIGHT AND WIDTH OF THE INPUT IMAGE, RESPECTIVELY.

Convolution	Norm	Activation	Output Size
$64 \times 7 \times 7$ Conv S1 P3	CBN	ReLU	$64 \times H \times W$
$128 \times 4 \times 4$ Conv S2 P1	CBN	ReLU	$128 \times \frac{H}{2} \times \frac{W}{2}$
$256 \times 4 \times 4$ Conv S2 P1	CBN	ReLU	$256 \times \frac{H}{4} \times \frac{W}{4}$
$256 \times 3 \times 3$ Res S1 P1	CBN	ReLU	$256 \times \frac{H}{4} \times \frac{W}{4}$
$256 \times 3 \times 3$ Res S1 P1	CBN	ReLU	$256 \times \frac{H}{4} \times \frac{W}{4}$
$256 \times 3 \times 3$ Res S1 P1	CBN	ReLU	$256 \times \frac{H}{4} \times \frac{W}{4}$
$256 \times 3 \times 3$ Res S1 P1	CBN	ReLU	$256 \times \frac{H}{4} \times \frac{W}{4}$
$256 \times 3 \times 3$ Res S1 P1	CBN	ReLU	$256 \times \frac{H}{4} \times \frac{W}{4}$
$256 \times 3 \times 3$ Res S1 P1	CBN	ReLU	$256 \times \frac{H}{4} \times \frac{W}{4}$
$128 \times 4 \times 4$ TrConv S2 P1	BN/IN	ReLU	$128 \times \frac{H}{2} \times \frac{W}{2}$
$64 \times 4 \times 4$ TrConv S2 P1	BN/IN	ReLU	$64 \times H \times W$
$3 \times 7 \times 7$ TrConv S1 P3	/	Tanh	$3 \times H \times W$

From Eq. 21, we learn that the mean value after BN relates to the input \mathbf{x} and minibatch.

As for instance normalization, it violates the diversity criterion.

$$E[\text{IN}(z_r)] = E\left[\frac{z_r - E[z_r]}{\sqrt{\text{Var}[z_r]}}\right] = \frac{E[z_r] - E[z_r]}{\sqrt{\text{Var}[z_r]}} = 0. \quad (22)$$

After applying central biasing, these normalization operations will meet the *design criteria*.

$$\begin{aligned} E[\text{CBN}(y_r, \vec{c})] &= E[\text{Norm}(y_r) - E[\text{Norm}(y_r)] + b_r(\vec{c})] \\ &= E[\text{Norm}(y_r)] - E[E[\text{Norm}(y_r)]] + E[b_r(\vec{c})] \\ &= E[b_r(\vec{c})]. \end{aligned} \quad (23)$$

For specific normalizations BN and IN, CBN can be simplified as CBBN and CBIN respectively:

$$\text{CBBN}(y_r, \vec{c}) = \frac{y_r - E[y_r]}{\sqrt{\text{Var}[\mathbf{Y}_r]}} + b_r(\vec{c}), \quad (24)$$

$$\text{CBIN}(y_r, \vec{c}) = \frac{y_r - E[y_r]}{\sqrt{\text{Var}[y_r]}} + b_r(\vec{c}). \quad (25)$$

It should be noted that CBBN eliminates the instance mean $E[y_r]$ instead of batch mean $E[\mathbf{Y}_r]$ and the variance of the output depends on the batch instead of instances like CBIN.

B. Central Biasing Generator

Instead of spatial replicating and concatenating into the inputs, we inject the latent code into the normalization layers by replacing traditional normalization with central biasing normalization, as shown in Fig. 6. We adapt the common encoder-decoder architecture [3], [8], [33] to build the generator, which contains two stride-2 convolution layers for downsampling, six residual blocks [34] and two stride-2 transposed convolution layers for upsampling. The normalization layers in the downsampling and residual blocks are replaced with central biasing

normalization layers to build a multi-mapping generator, which we refer to as the central biasing generator. The network architecture is shown in Table II.

VI. EXPERIMENTS

As mentioned in the above sections, the multi-mapping tasks can be classified as multi-modal tasks and multi-domain tasks. We choose the state-of-the-art models for each task as our baselines. Specifically, we adopt BicycleGAN [9] and pix2pix [1] for multi-modal tasks and StarGAN [8] for multi-domain translation tasks.

A. Multi-domain Translation

1) *Dataset*: Facial attribute transfer is a typical multi-domain translation problem. We randomly select 2,000 images from 202,599 face images in CelebA dataset [35] of celebrities as a test set and retain the rest of images for a training set. Then, we crop the images to 178×178 , and resize them to 128×128 . Seven facial attributes are selected to train the multi-domain transform models: hair color (black, blond, brown), gender (male/female), and age (young/old).

2) *Baseline*: To model multi-domain mappings with a single model, StarGAN introduces the auxiliary classifier [24] for the discriminator. Since StarGAN uses the attribute label as the latent code \vec{c} , the latent space is discrete and the state of \vec{c} is limited.

3) *Metrics*: To judge the specific domains image translation capabilities, we compare the classification accuracy of facial attributes on synthesized images. We use the ResNet-18 [34] which is pre-trained on the ImageNet dataset [36], and fine-tune it for multi-label classification on the CelebA dataset (10-fold cross validation in training set). We use the same training set for each image translation model and translate all possible combinations (12 domain of facial attributes) from the unseen test images.

B. Multi-modal Translation

1) *Datasets*: We perform the evaluation on several multi-model translation tasks, including edge2photo [37], [38], label2photo [39], night2day [40]. We resize all of the images to 128×128 .

2) *Baseline*: To model the distribution of possible outputs in a conditional generative modeling setting, BicycleGAN combines the VAE-GAN [25] and LR-GAN [12], [26], [27] objectives for encouraging a bijective mapping between the latent and output spaces. Since BicycleGAN use the encoder with a Gaussian assumption to extract the latent code \vec{c} , the latent space is continuous and the state of \vec{c} is varied. To further compare the effect between LCI and CBN, we also remove the encoder of BicycleGAN and use the noise vector as the latent code. Without incentive for the generator to make use of latent code, BicycleGAN degenerates into pix2pix [1].

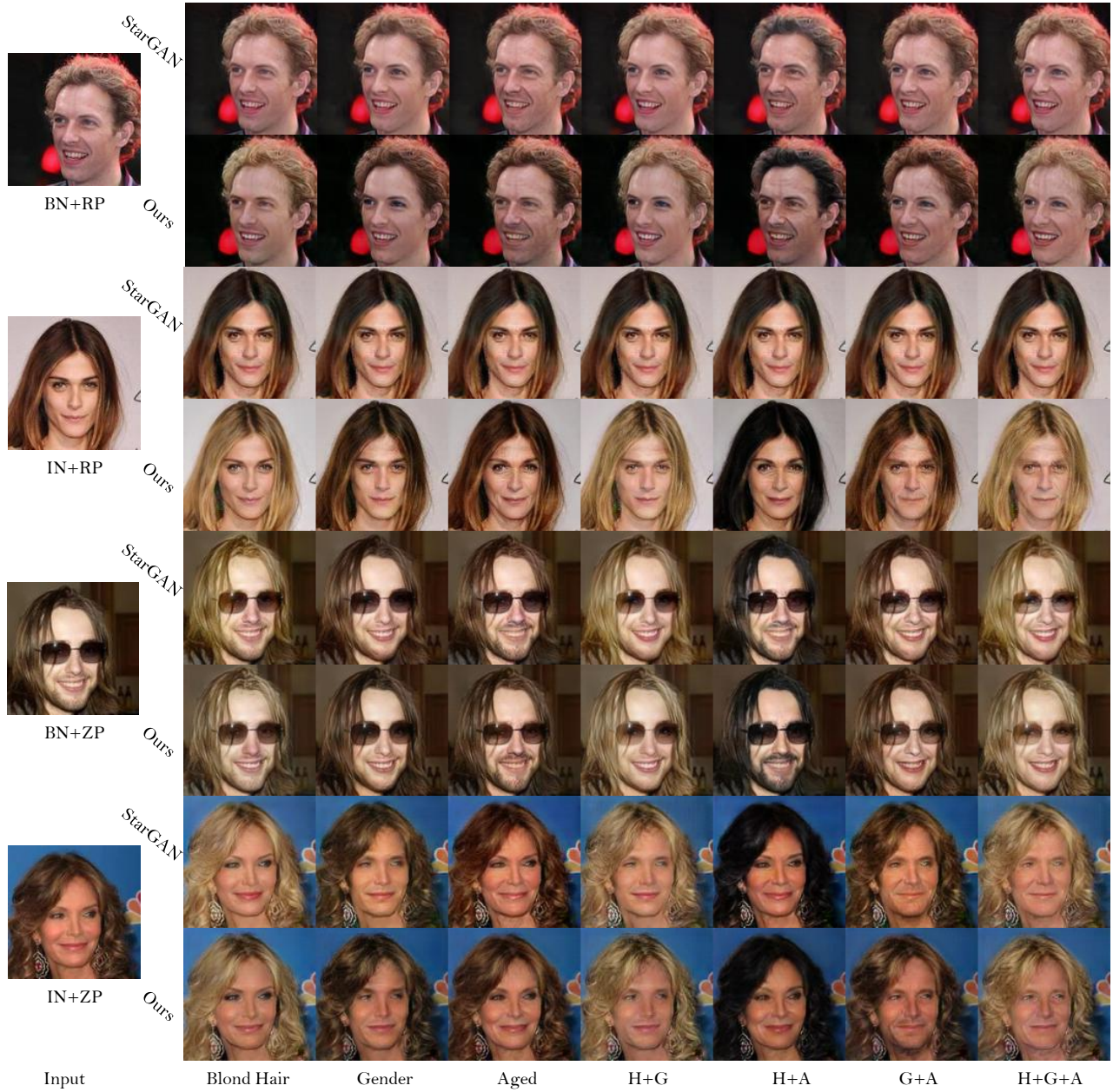


Fig. 7. Facial attribute transfer results. The first column show the input images, next three columns show the single attribute transform results, and the rest of columns show the multi-attribute transfer results. H: Hair color, G: Gender, A: Aged.

TABLE III
THE CLASSIFICATION ACCURACY FOR FACIAL ATTRIBUTE TRANSFER RESULTS.

Method	Hair color	Gender	Aged	Average
BN+RP StarGAN	70.90	61.16	61.57	64.54
Ours	81.93	68.00	63.21	71.05
IN+RP StarGAN	33.33	50.00	50.00	44.44
Ours	96.46	88.55	86.05	90.36
BN+ZP StarGAN	84.25	79.53	66.09	76.62
Ours	88.63	76.32	67.76	77.57
IN+ZP StarGAN	95.25	88.38	86.05	89.89
Ours	95.74	90.20	86.11	90.68
Real images	91.56	97.25	88.74	92.52

TABLE IV
THE PERCEPTUAL DISTANCE FOR EDGES2PHOTOS AND LABEL2PHOTOS TASKS.

Method	edge→photo	label→photo	Average
BN+RP BicycleGAN	0.069	0.629	0.349
Ours	0.867	1.499	1.183
IN+RP BicycleGAN	1.025	1.027	1.026
Ours	1.652	1.417	1.535
BN+ZP BicycleGAN	0.492	1.281	0.887
Ours	0.754	1.641	1.198
IN+ZP BicycleGAN	1.106	1.318	1.212
Ours	1.637	1.562	1.599
Real images	3.481	3.233	3.357



Fig. 8. Edge2Photo results. The first column shows the input images and the remaining columns are the results transfer from sample latent code.

TABLE V
THE CONSISTENCY SCORE FOR EDGE2PHOTO AND LABEL2PHOTO TASKS.

Method		edge→photo	label→photo	Average
BN+RP	BicycleGAN	0.906	0.848	0.877
	Ours	0.951	0.858	0.905
IN+RP	BicycleGAN	0.949	0.852	0.901
	Ours	0.966	0.868	0.917
BN+ZP	BicycleGAN	0.939	0.862	0.901
	Ours	0.951	0.864	0.908
IN+ZP	BicycleGAN	0.952	0.867	0.910
	Ours	0.966	0.867	0.917

3) *Metrics*: We compare the diversity of different models by computing averaged perceptual distance in feature space. As suggested in [9], we use the cosine similarity (CosSim) to evaluate the distance in the feature space of the VGG-16 network [41] pre-trained in ImageNet. We average across

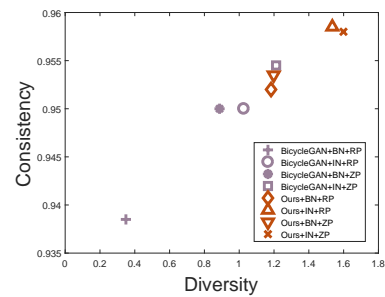


Fig. 9. Consistency vs Diversity. We measure diversity using perception distance, and consistency using l_1 reconstruction on the edge2photo and label2photo tasks.

spatial dimensions and sum across the five convolution layers preceding the pool layers. As in Zhu *et al.* [9], the perceptual

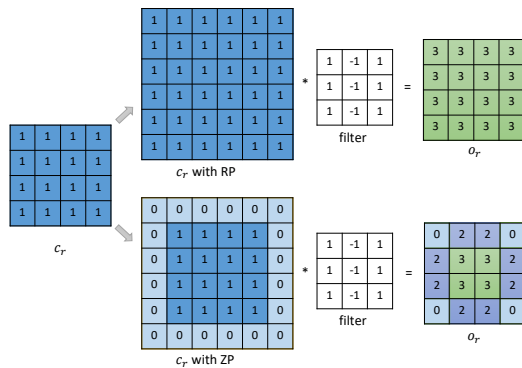


Fig. 10. Different padding operations. The first column is the source latent code channel c_r . The first row in the rest of the columns is the convolution with reflection-padding, and the second row is the convolution with zero-padding.

distance is defined as $(5.0 - \sum_{i=1}^5 \text{CosSim}_i)$. The larger the perceptual distance, the greater the difference between two images. To evaluate the diversity of different models, we randomly sample an input image and use a pair of random latent code to generate images. Then, we compute the average distance between 2,000 pairs of generated images. Besides, we use the latent code encoded by ground truth to indicate the image generation, and to calculate the l_1 reconstruction loss to measure the consistency of BicycleGAN. To be more intuitive, the consistency is defined as $(1.0 - \|G(\text{Enc}(y), x) - y\|_1)$, where x and y are the input and target images, Enc is the encoder, and G represents the generator. The larger the consistency score, the greater the consistency of model.

C. Verification of Potential Problems

As discussed in Section IV, the existing latent code injection model has some potential problems when modeling multi-mapping. But in the existing works [8], [9], why do similar convolution pipelines with instance normalization still work? The reason is that these networks introduce zero-padding (ZP) before the convolution operation, which aims to control the spatial size of the output volume. After zero-padding, the latent code channel of the input volume is no longer a constant plane but has a circle of zero boundaries. Through convolutional operation, the latent code convolution output o_r in Eq. 4 is not a constant feature map. The convolution activation boundaries give the possibility of the feature maps of keeping diversity in non-boundary areas after instance normalization. However, such problems still exist if we unequip the zero-padding or use other padding strategy, such as reflection-padding (RP). To validate the problems, we replace ZP with RP in StarGAN and BicycleGAN during the following experiments.

1) *Impaired Consistency of BN*: To verify the mapping inconsistency of batch normalization, we replace the original generator with the proposed CBG model under the settings of CBBN. The qualitative comparison results are shown in Fig. 7, 8. To quantitatively analyze the model performance, we test the diversity and classification error of these models, as shown in Table III, IV. We obtain quantitative results that comply with qualitative performance. Both the common latent

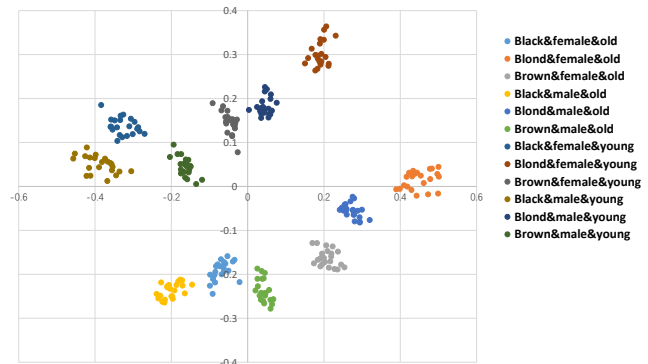


Fig. 11. The results of k-means clustering from 2 dimensional statistical data. Different colors represent different mappings indicated by latent code.

code injection models produce realistic outputs but lose output diversity. Conversely, CBG produces various outputs while maintaining realistic. The main difference between common LCI models and CBG is the mean value of feature maps after normalization. The mapping inconsistency of BN seriously affects the performance of the network. During training time, the network can hardly learn the deterministic mapping since the feature mean of same mapping is always changing. After correcting the inconsistency by CBN, the mapping indicated by the latent code is stable.

2) *Impaired Diversity of IN*: In order to explore the mapping elimination of instance normalization, we equip instance normalization in BicycleGAN and StarGAN. Meanwhile, we use CBG as a comparison under CBBN settings. We employ the original implementation of BicycleGAN with the UNet generator [42] which does not equip normalization in the first convolution layer. Since the effect of latent code is eliminated after IN, StarGAN fails to perform domain translation as shown in Fig. 7. Without normalization of the first convolution, BicycleGAN can retain the diversity indicated by latent code, as shown in Fig. 8. But the visual quality is not very satisfactory. It suggests that discarding normalization is not a good idea to retain diversity in the deep network. Under the similar settings, CBG presents more satisfactory results and produces a higher diversity score.

D. Discussion

1) *Translation Consistency*: Besides the diversity of different mappings, the consistency of same mapping should be considered for multi-mapping models. For StarGAN, it can use the domain classification accuracy to as a metric, as shown in Table III. For BicycleGAN, we use the reconstruction loss to measure the consistency of the model, as shown in Table V. Along with the diversity results in Table IV, we can observe that the consistency and diversity of CBG outperform to BicycleGAN, as shown in Fig. 9. More consistency results generated by CBG are shown in Fig. 15.

2) *Role of Padding*: To study the role of padding strategy for multi-mapping model, we compare the performance of models under different padding settings. As the qualitative results in Fig. 7, 8 show, we observe that ZP mode is more

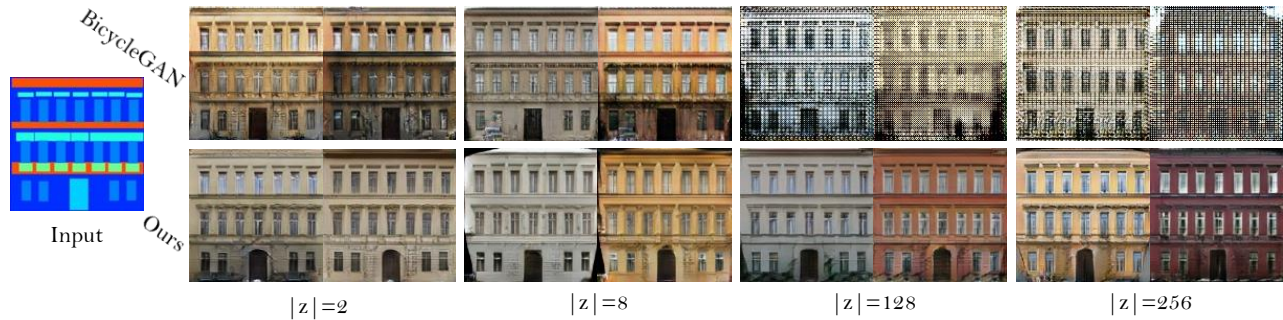


Fig. 12. Label2photo results with varying length of the latent code. Larger $|z|$ can encode more information for expressive results but is not conducive to BicycleGAN output densely fill results. The performance of CBG is stable when $|z|$ is large enough.

TABLE VI

THE PERCEPTUAL DISTANCE FOR CBG WITH DIFFERENT CONSTRAINT FUNCTIONS.

Constraint	edge→photo	label→photo	Average
None	1.577 ^a	1.609	1.593
Tanh	1.637	1.562	1.600
Sigmoid	1.427	1.166	1.297

^a The results were calculated from the generated images before mode collapse.

TABLE VII

GENERATOR PARAMETERS WITH DIFFERENT LENGTH OF LATENT CODE.

Base model	BicycleGAN	CBG
	39.9M	8M
$ z = 2$	+78K	+6.9K
$ z = 8$	+312K	+27.5K
$ z = 128$	+4.9M	+440K
$ z = 256$	+9.75M	+880K

diverse and realistic than RP mode for traditional LCI. The observation is also consistent with the results of quantitative analysis. Let us revisit the padding strategy shown in Fig. 10. As discussed in the previous sections, latent code just provides a constant offset in RP mode, so the mapping inconsistency and mapping elimination problems still exist. For ZP mode, the convolution of latent code provides the feature map which contains non-constant boundaries and a constant center region. Therefore, the network has the ability to control the distribution of features for different mappings after normalization. Since the feature mean is normalized to zero after IN, the common LCI model with ZP is inconsistent with our *diversity criteria* on the surface. But apart from the non-constant boundaries, the feature map of latent code does provide a constant offset. We think the key to distinguish different mappings is also the mean value in non-boundary feature regions.

After testing the StarGAN under the settings of IN+ZP, we find the feature mean and target mapping are strongly related. We first sample the feature maps z which are the normalization output with a latent code injection convolution operation. In the test images with 12 conversions, the feature mean is calculated without considering the boundary area affected by padding operation. To reduce the computational complexity, we use principal component analysis (PCA) to reduce the dimension of the statistical mean feature maps. While retaining 96% variance, we reduce the data from 64 to 6 dimensions. After performing k-means (k=12) clustering in the low dimensional data, we find that each cluster represents a kind of mapping. We reduce the data dimension to 2 using PCA for visualization, as shown in Fig. 11.

This phenomenon implies that zero padding of LCI model helps the model to perform multi-mapping by controlling the distribution of feature. The role of ZP in traditional LCI is

similar to central biasing normalization. Since there is no need to optimize redundant parameters of V in Eq. 3, CBG optimizes target mapping more directly.

3) *Range of Bias*: In our proposed CBN, we apply \tanh function to stabilize the output distribution of normalization in Eq. 20. Here we focus on the impact of different bias ranges on performance. We extend the range of bias by removing \tanh function, and narrow the range by replacing \tanh with sigmoid . We test CBN with these strategies in the BicycleGAN based CBG and compare with the default setting (CBIN&ZP). As show in Table VI, we find that sigmoid is inferior to \tanh in diversity performance. It implies that narrow range of bias will limit the representation of network. This finding is further validated when we remove constraint function to expand the range of bias in the label→photo task. But we also observe that removing constraint function will lead to the instability in training stage, since the feature distribution is unbounded. This phenomenon is obvious in edge→photo task since its large amount of data and style. In this task, we find that the generator is easy to collapse when we remove the constraint of bias. So we suggest to use \tanh function to constrain the range of bias while maintaining the representation of network.

4) *Effects of Latent Code Length*: As in Zhu *et al.* [9], we explore the effect of latent code length on model performance. Under varying numbers of dimensions of latent codes $\{2, 8, 128, 256\}$, we test the default BicycleGAN, which uses IN and ZP, and CBG with similar settings. Similar the results of Zhu *et al.* [9], a high-dimensional latent code can potentially encode more information for image generation at the cost of making sampling quite difficult for the common LCI model. CBG shows stable performance when the dimension of latent code is high enough, as shown in Fig. 12. The reason behind that is CBN provides a more stable distribution with range

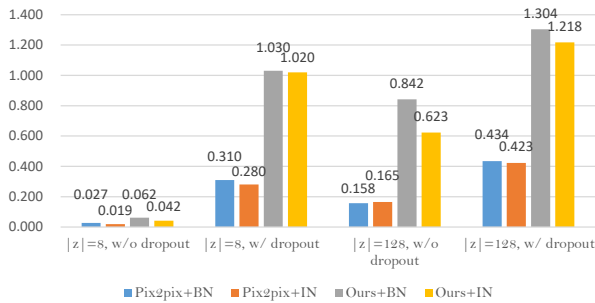


Fig. 13. The perceptual distance of pix2pix based models. We compare diversity results on the `label2photo` across different construction strategies.

constraint. In addition, CBG is low cost for increasing the dimension of latent code. Table VII shows the number of generator parameters compared with BicycleGAN and CBG. Due to replication of latent code in the common LCI model, the convolutional parameters for latent code (convolution matrix \mathbf{V} in Eq. 3) are redundant. For a fair comparison, we just use the suggested latent code dimension 8 [9] in above experiments.

5) *CBN without Incentive*: To further explore the effectiveness of CBN when it lacks incentive to make use of latent code, we randomly sample Gaussian noise as the latent code inject to pix2pix [1], which can be considered as the degradation of BicycleGAN. Similar to [1], we apply dropout with rate of 50% to the generator (Convolution-Norm-Dropout-ReLU) to increase the stochasticity in the output. Besides, we also extend the dimension of latent code to reinforce its effect. The diversity results are show in Fig. 13, and the qualitative comparison are presented in Fig. 14. Similar to the results in [1], [9], we observe that injecting noise to the original pix2pix does not produce large variation. This situation has not improved even though we applied dropout and extended the dimension of latent code. The same results also appear when we directly replace the generator in pix2pix with CBG. After applying dropout operation, we observe that the diversity score is improved by introducing stochasticity in the image structure. By extending the dimension of latent code, we find that the number of the output styles is increased and the diversity score is also improved. When we apply both strategies to CBG, we get the best diversity performance in the pix2pix based model.

6) *CBBN and CBIN*: In our *design criteria*, we assume that the crucial statistics of multi-mapping model is the mean value of feature maps. There is no constraint on other statistical properties, such as variance. The difference between of CBBN and CBIN is actually the feature variance of the same mapping. After CBBN, the statistical variance of features in the same mapping is not identical since it uses the variance of the batch. After CBIN, the statistical variance of features is normalized to 1 since it uses the variance of instance. With incentive to make use latent code, CBIN presents a higher diversity score than CBBN since it uses the stable variance in the training stage. When we remove incentive, the latent code can be consider as the noise to the network. In these cases, CBBN outperforms CBIN since the minibatch variance is more stable than the

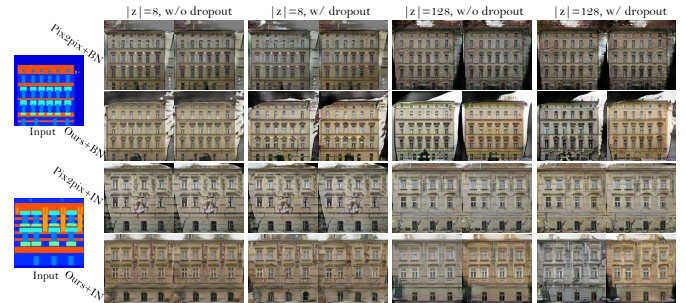


Fig. 14. Qualitative comparison of pix2pix based models. Each image pair generated by same input and different noises z .

instance variance. This indicates that a stable data distribution is essential for the network to learn the translation mapping.

VII. CONCLUSIONS

In this paper, we study the latent code injection in multi-mapping convolution neural network. By decomposing the convolution output, we show that the latent code provides different offsets to affect the statistical means of output feature maps. With further analysis, we find the *mapping inconsistency* and *mapping indistinguishability* problems of existing methods. To overcome these problems, we propose the *consistency within diversity criteria* as a guide to designing the multi-mapping model. Based on the *design criteria*, we propose central biasing normalization to replace the existing latent code injection. Specifically, we design a central biasing generator for multi-mapping image generation.

Through experiments, our method presents more diverse results than LCI model in the similar settings. Since the potential problems discussed above, LCI model almost lose all diversity when it equips reflection padding. Although zero padding can help maintain the diversity of LCI model, it limits the flexibility of model design and requires more parameters than central biasing normalization. By constraining the range of bias, central biasing normalization provides a stable distribution of activation values. This constraint allows the generator to learn the stable mappings without regard to the dimension of latent code. In the meanwhile, we find that high-dimensional latent code is beneficial to increase the output diversity when the generator equips CBN. This conclusion still holds even there is no incentive for the generator to make use of latent code.

Not only central biasing normalization can be used as an alternative for latent code injection in image translation, it also provides a simple method to extend the representation ability of convolutional neural networks. In our future work, we will investigate whether central biasing normalization can help with domain adaptation if we inject the domain information for the network. Besides, the bias provided by central biasing normalization is consistent for the entire feature map, even though the transform is non-global, *e.g.* facial expression transform. It seems possible to introduce some local operations to improve the model performance for the local transformation. Finally, we believe that this work is valuable for studying the multi-mapping translation. Further exploration will allow

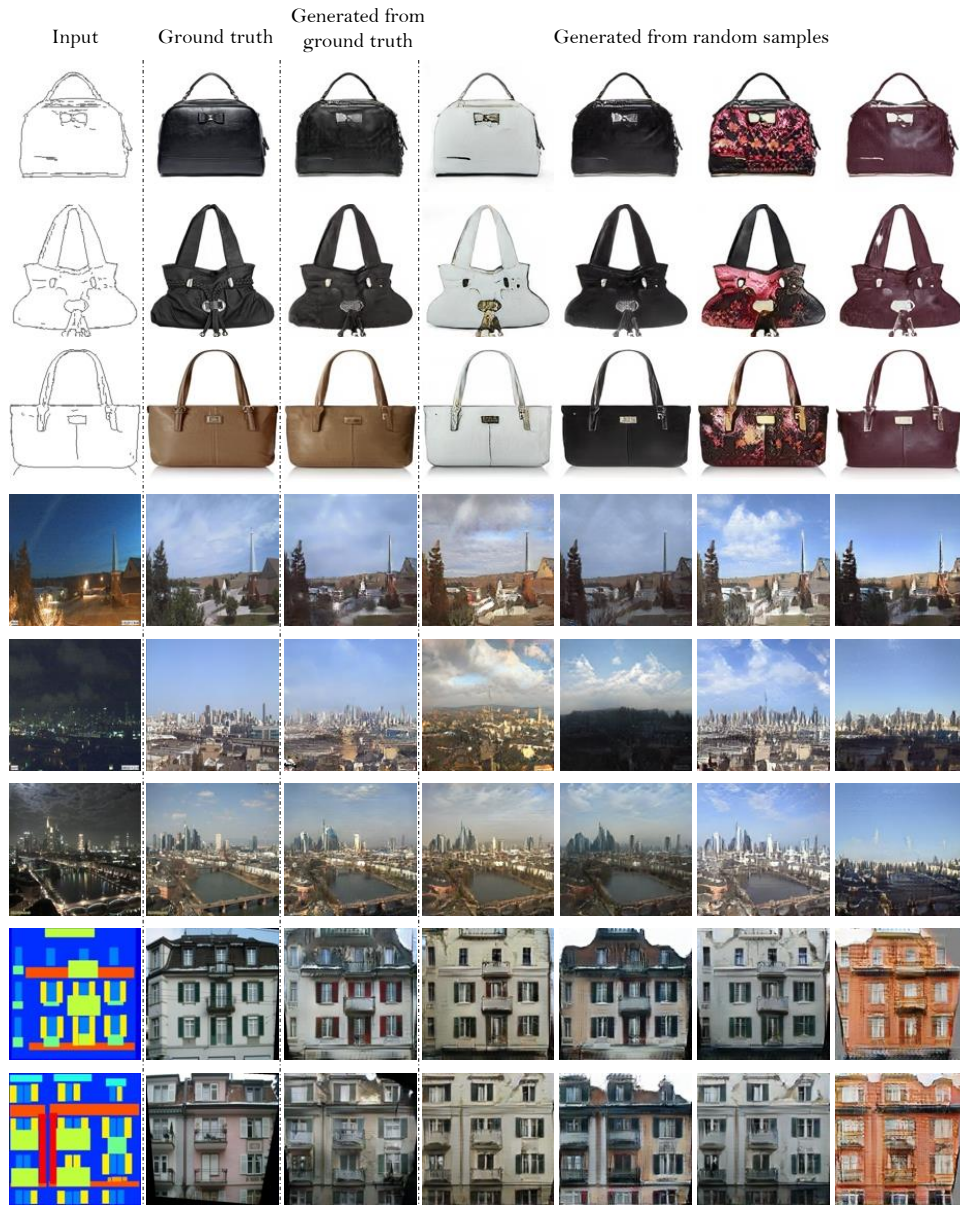


Fig. 15. Consistency results of multi-modal translation on `edge2photo`, `night2day` and `label2photo` under CBIN+RP settings. The left column contains the input images. The second shows the ground truth outputs. The third shows the generated outputs with latent code encoded from ground truth. The rest of the columns show the generated outputs using different latent code. The latent code is fixed in each column in each task. Therefore, results from the same column have similar style.

the proposed method more universal and effective in different applications.

REFERENCES

[1] P. Isola, J.-Y. Zhu, T. Zhou, and A. A. Efros, “Image-to-image translation with conditional adversarial networks,” in *Computer Vision and Pattern Recognition (CVPR), 2017 IEEE Conference on*, 2017.

[2] R. Zhang, P. Isola, and A. A. Efros, “Colorful image colorization,” *European Conference on Computer Vision*, 2016.

[3] J.-Y. Zhu, T. Park, P. Isola, and A. A. Efros, “Unpaired image-to-image translation using cycle-consistent adversarial networks,” in *Computer Vision (ICCV), 2017 IEEE International Conference on*, 2017.

[4] Z. Yi, H. Zhang, P. Tan, and M. Gong, “Dualgan: Unsupervised dual learning for image-to-image translation,” in *IEEE International Conference on Computer Vision*, 2017, pp. 2868–2876.

[5] T. Kim, M. Cha, H. Kim, J. K. Lee, and J. Kim, “Learning to discover cross-domain relations with generative adversarial networks,” in *International Conference on Machine Learning*, 2017, pp. 1857–1865.

[6] M.-Y. Liu, T. Breuel, and J. Kautz, “Unsupervised image-to-image translation networks,” in *Advances in Neural Information Processing Systems*, 2017, pp. 700–708.

[7] G. Lample, N. Zeghidour, N. Usunier, A. Bordes, L. Denoyer *et al.*, “Fader networks: Manipulating images by sliding attributes,” in *Advances in Neural Information Processing Systems*, 2017, pp. 5969–5978.

[8] Y. Choi, M. Choi, M. Kim, J.-W. Ha, S. Kim, and J. Choo, “Stargan: Unified generative adversarial networks for multi-domain image-to-image translation,” *arXiv preprint arXiv:1711.09020*, 2017.

[9] J.-Y. Zhu, R. Zhang, D. Pathak, T. Darrell, A. A. Efros, O. Wang, and E. Shechtman, “Toward multimodal image-to-image translation,” in *Advances in Neural Information Processing Systems 30*, 2017.

[10] I. Goodfellow, J. Pouget-Abadie, M. Mirza, B. Xu, D. Warde-Farley, S. Ozair, A. Courville, and Y. Bengio, “Generative adversarial nets,” in *Advances in neural information processing systems*, 2014, pp. 2672–

- 2680.
- [11] X. Mao, Q. Li, H. Xie, R. Y. Lau, Z. Wang, and S. P. Smolley, "Least squares generative adversarial networks," in *2017 IEEE International Conference on Computer Vision (ICCV)*. IEEE, 2017, pp. 2813–2821.
 - [12] X. Chen, Y. Duan, R. Houthoofd, J. Schulman, I. Sutskever, and P. Abbeel, "Infogan: Interpretable representation learning by information maximizing generative adversarial nets," in *Advances in Neural Information Processing Systems*, 2016, pp. 2172–2180.
 - [13] M. Arjovsky, S. Chintala, and L. Bottou, "Wasserstein generative adversarial networks," in *International Conference on Machine Learning*, 2017, pp. 214–223.
 - [14] I. Gulrajani, F. Ahmed, M. Arjovsky, V. Dumoulin, and A. C. Courville, "Improved training of wasserstein gans," in *Advances in Neural Information Processing Systems*, 2017, pp. 5769–5779.
 - [15] A. Radford, L. Metz, and S. Chintala, "Unsupervised representation learning with deep convolutional generative adversarial networks," *ICLR*, 2016.
 - [16] D. Pathak, P. Krahenbuhl, J. Donahue, T. Darrell, and A. A. Efros, "Context encoders: Feature learning by inpainting," in *Proceedings of the IEEE Conference on Computer Vision and Pattern Recognition*, 2016, pp. 2536–2544.
 - [17] C. Ledig, L. Theis, F. Huszár, J. Caballero, A. Cunningham, A. Acosta, A. Aitken, A. Tejani, J. Totz, Z. Wang *et al.*, "Photo-realistic single image super-resolution using a generative adversarial network," in *Computer Vision and Pattern Recognition (CVPR), 2017 IEEE Conference on*, 2017.
 - [18] S. Reed, Z. Akata, X. Yan, L. Logeswaran, B. Schiele, and H. Lee, "Generative adversarial text to image synthesis," in *International Conference on Machine Learning*, 2016, pp. 1060–1069.
 - [19] Y. Tian, X. Peng, L. Zhao, S. Zhang, and D. N. Metaxas, "Cr-gan: Learning complete representations for multi-view generation," *International Joint Conference on Artificial Intelligence*, 2018.
 - [20] A. Brock, T. Lim, J. M. Ritchie, and N. Weston, "Neural photo editing with introspective adversarial networks," *ICLR*, 2017.
 - [21] M. Mirza and S. Osindero, "Conditional generative adversarial nets," *arXiv preprint arXiv:1411.1784*, 2014.
 - [22] D. P. Kingma and M. Welling, "Auto-encoding variational bayes," *ICLR*, 2014.
 - [23] M.-Y. Liu and O. Tuzel, "Coupled generative adversarial networks," in *Advances in neural information processing systems*, 2016, pp. 469–477.
 - [24] A. Odena, C. Olah, and J. Shlens, "Conditional image synthesis with auxiliary classifier gans," *arXiv preprint arXiv:1610.09585*, 2016.
 - [25] A. B. L. Larsen, S. K. Sønderby, H. Larochelle, and O. Winther, "Autoencoding beyond pixels using a learned similarity metric," in *33rd International Conference on Machine Learning*, 2016.
 - [26] J. Donahue, P. Krähenbühl, and T. Darrell, "Adversarial feature learning," *ICLR*, 2016.
 - [27] V. Dumoulin, I. Belghazi, B. Poole, O. Mastropietro, A. Lamb, M. Arjovsky, and A. Courville, "Adversarially learned inference," *ICLR*, 2016.
 - [28] J. Cong and B. Xiao, "Minimizing computation in convolutional neural networks," in *International conference on artificial neural networks*. Springer, 2014, pp. 281–290.
 - [29] S. Ioffe and C. Szegedy, "Batch normalization: Accelerating deep network training by reducing internal covariate shift," in *International conference on machine learning*, 2015, pp. 448–456.
 - [30] H. Shimodaira, "Improving predictive inference under covariate shift by weighting the log-likelihood function," *Journal of statistical planning and inference*, vol. 90, no. 2, pp. 227–244, 2000.
 - [31] D. Ulyanov, A. Vedaldi, and V. Lempitsky, "Improved texture networks: Maximizing quality and diversity in feed-forward stylization and texture synthesis," in *Computer Vision and Pattern Recognition (CVPR), 2017 IEEE Conference on*, 2017.
 - [32] X. Huang and S. Belongie, "Arbitrary style transfer in real-time with adaptive instance normalization," in *ICCV*, 2017.
 - [33] J. Johnson, A. Alahi, and L. Fei-Fei, "Perceptual losses for real-time style transfer and super-resolution," in *European Conference on Computer Vision*. Springer, 2016, pp. 694–711.
 - [34] K. He, X. Zhang, S. Ren, and J. Sun, "Deep residual learning for image recognition," in *Proceedings of the IEEE conference on computer vision and pattern recognition*, 2016, pp. 770–778.
 - [35] Z. Liu, P. Luo, X. Wang, and X. Tang, "Deep learning face attributes in the wild," in *Proceedings of the IEEE International Conference on Computer Vision*, 2015, pp. 3730–3738.
 - [36] O. Russakovsky, J. Deng, H. Su, J. Krause, S. Satheesh, S. Ma, Z. Huang, A. Karpathy, A. Khosla, M. Bernstein *et al.*, "Imagenet large scale visual recognition challenge," *International Journal of Computer Vision*, vol. 115, no. 3, pp. 211–252, 2015.
 - [37] A. Yu and K. Grauman, "Fine-grained visual comparisons with local learning," in *Proceedings of the IEEE Conference on Computer Vision and Pattern Recognition*, 2014, pp. 192–199.
 - [38] J.-Y. Zhu, P. Krähenbühl, E. Shechtman, and A. A. Efros, "Generative visual manipulation on the natural image manifold," in *European Conference on Computer Vision*. Springer, 2016, pp. 597–613.
 - [39] R. Tyleček and R. Šára, "Spatial pattern templates for recognition of objects with regular structure," in *German Conference on Pattern Recognition*. Springer, 2013, pp. 364–374.
 - [40] P.-Y. Laffont, Z. Ren, X. Tao, C. Qian, and J. Hays, "Transient attributes for high-level understanding and editing of outdoor scenes," *ACM Transactions on Graphics (proceedings of SIGGRAPH)*, vol. 33, no. 4, 2014.
 - [41] K. Simonyan and A. Zisserman, "Very deep convolutional networks for large-scale image recognition," *Computer Science*, 2014.
 - [42] O. Ronneberger, P. Fischer, and T. Brox, "U-net: Convolutional networks for biomedical image segmentation," in *International Conference on Medical image computing and computer-assisted intervention*. Springer, 2015, pp. 234–241.